IEEE Open Journal of Control Systems

Received 22 November 2025; revised 6 February 2026; accepted 23 February 2026. Date of publication 2 March 2026; date of current version 16 March 2026. Recommended by Senior Editor Peter Seiler.

Digital Object Identifier 10.1109/OJCSYS.2026.3669038

On the Equivalence of Sensory and Incremental Nonlinear Dynamic Inversion

S. HAFNER [1,2] (Graduate Student Member, IEEE), T. DE PONTI [2], AND E. SMEUR [2]

[1]Institute of Flight System Dynamics, Technical University of Munich, 85748 Garching, Germany
[2]Faculty of Aerospace Engineering, Delft University of Technology, HS 2629 Delft, The Netherlands

CORRESPONDING AUTHOR: S. HAFNER (e-mail: simon.hafner@tum.de).

The work of Simon Hafner was supported by scholarship from Munich Aerospace e.V. This work was supported in part by the Royal Dutch Navy and in part by the Dutch Coast Guard. This initiative aims to foster collaboration and innovation in maritime endeavors.

ABSTRACT In the aerospace control domain, Nonlinear Dynamic Inversion (NDI)-based control laws are widely spread. As a variation to Incremental Nonlinear Dynamic Inversion (INDI), the sensory Nonlinear Dynamic Inversion (sNDI) method was recently developed. Both methods rely on replacing model knowledge with sensor measurements. However, the methods differ in how the pseudo-controls are allocated: INDI allocates them incrementally, while sNDI allocates them globally, with corresponding advantages and disadvantages. While INDI requires a restoring mechanism in the control allocation due to path dependency issues in overactuated nonlinear systems, sNDI does not experience this problem. In addition to the comparison, the paper demonstrates that both methods lead to identical results if restoring is applied in the control allocation of INDI. Even though sNDI and INDI with restoring can lead to limit cycles for theoretical non-linear overactuated systems, the practical applicability of this approach to transition electrical vertical take-off and landing vehicles (eVTOL) is demonstrated in flight tests of the Variable Skew Quad Plane.

INDEX TERMS Aerospace, feedback linearization, flight control, nonlinear output feedback, nonlinear systems and control.

I. INTRODUCTION

Incremental Nonlinear Dynamic Inversion (INDI) has gained popularity in the flight control community over the recent decade. It stems from the well-known Nonlinear Dynamic Inversion (NDI) control method. The incremental approach can reduce model-dependency compared to the NDI approach, because a measurement replaces the state-dependent term. The remaining required model knowledge lies in the input function or control effectiveness. Due to the reduced model dependency,INDI can be applied to various types of vehicles with reduced adaptation effort. INDI has been successfully applied to various types of vehicles like fighter aircraft [1], [2], [3], lift and cruise vehicles [4], [5], and multicopters [6], [7].

Generally, INDI can be differentiated into sensor-based and model-based INDI [8], [9]. As the name suggests, sensor-based INDI replaces the model knowledge directly with measurements, whereas model-based INDI relies on an onboard plant model (OBPM) and is therefore closely related to the NDI control structure. Hybrid INDI is a mixed approach that combines measurements and model data [8].

In classic INDI, heterogeneous actuator dynamics can lead to cross-coupling effects and imperfect inversion. To avoid this issue, Raab et al. [4] proposed the extended INDI approach, which inverts the actuator dynamics. A feedforward through the extension to a higher-order reference model by Steffensen et al. [10] then propose the Actuator Nonlinear Dynamic Inversion (ANDI) method, which consistently accounts for the state-dependent term in the feedback path. The ANDI controller has been successfully applied on a skewing wing-drone [5].

The standard structure of INDI computes a pseudo-control increment $\Delta \boldsymbol{\nu}$, which is then allocated to input increments $\Delta \boldsymbol{u}$ by the control allocation (CA) [11]. To arrive at the actual input, the increment is added to the measured or estimated $\boldsymbol{u}_0$. This allows the use of the local linearization of the control effectiveness, which is the primary advantage over global linear allocation for nonlinear control effectiveness, as shown in [12, Fig. 4]. When using a pseudoinverse-based or quadratic programming (minimal least squares) allocation, the CA will minimize $\|\Delta \boldsymbol{u}\|_2$ or a weighted version [13].

This incremental control allocation (INCA) features several differences from global CA. One is the path dependency problem, which can lead to undesired effector usage in steady state conditions [13]. To overcome this issue, a process called *restoring* can be applied, which drives back the desired trim positions/inputs [13], [14]. A similar method is also referred to as null-space transition, which allows for more complex objectives [15]. The restoring method is a specific case of a general secondary objective that can be introduced into the control allocation solver [16]. The restoring can be applied either sequentially after the primary allocation, as in Sequential Least Squares (SLS) [16] or the null-space transition [15], or integrated in one control allocation problem, as in Weighted Least Squares (WLS) [17], [18]. When introducing a secondary objective based on global desired inputs for all control inputs, the control allocation in INDI becomes, by implication, a global allocation.

Recently, a new formulation of INDI control laws has emerged. This new control law performs control allocation at the global level, whereas in standard INDI it is usually incremental, optionally including a global secondary objective. The general formulation is first presented in [19], which references a not-yet-published publication. Later, the same authors name it sensory Nonlinear Dynamic Inversion (sNDI) in [20]. The name sNDI refers to the derivation from NDI by replacing the solely state-dependent term with a sensor measurement; see Section II. On the other hand, the same law can also be derived from the INDI approach, which relies on the difference between the desired pseudo-control and the measured pseudo-control. Therefore, sNDI can also be considered a part of the INDI family. Specifically, it also resembles the open (free) integration of the pseudo-control increment like INDI, but before the control allocation, not after. For the sake of short notation and due to the established term, this paper will refer to it as sNDI.

In [19], sNDI is presented for input-affine systems and used to control a tilt-wing vehicle in simulation. The approach is then extended to input non-affine systems in [20]. In non-affine systems, either a linearization similar to INDI would need to be applied, or a nonlinear optimization problem solved [20]. Further, Milz et al. [20] demonstrate how secondary objectives can be included in the unconstrained control allocation. The same approach is then applied to tandem tilt-wing electrical Vertical Take-Off and Landing vehicles (eVTOL) in simulation [21]. Mancinelli et al. [22] deploy sNDI with nonlinear control allocation to a dual-axis tilting rotor quad-plane

The sNDI law is also used as part of hybrid NDI laws, which mix model- and sensor-based pseudo-controls [23], [24]. The hybrid law was flight-tested on the Research Aircraft PH-LAB, a Cessna Citation II [23]. To solve the control allocation problem, a Taylor series expansion is again applied [24].

Depending on the use case, the sNDI has some advantages over INDI when a secondary global objective is included in the allocation. The sNDI control law allocates control inputs using global pseudo-control commands. When allocating the global pseudo-control to the global inputs, a pseudoinverse-based control allocation automatically minimizes the input norm $\|\boldsymbol{u}\|_2$. If the desired input is $\boldsymbol{u}_{\text{des}} = \boldsymbol{0}$, the secondary objective can also be omitted in SLS and WLS, while no path-dependency issue is expected. Therefore, sNDI has a lower computational effort compared to INDI in this case. If a different secondary objective is chosen, this advantage vanishes and the computational effort of sNDI may be even larger due to the additional matrix-vector multiplication in the feedback.

An additional benefit of the sNDI structure is that external disturbances and model uncertainty can be directly observed in the output space. This allows us to limit the maximum disturbance rejection per output, ensuring that the control effort spent on specific outputs can be restricted during flight phases where the allocation of other outputs is more critical. An example is the landing phase of an eVTOL, where it is crucial to control the roll and pitch attitudes, while heading is less important. Another benefit of the sNDI is the less complex synchronization and filtering effort [21].

The contributions of this paper are structured as follows. We provide two derivations of the sNDI law and thoroughly examine its behavior in comparison to INDI for various system types. Further, we prove that INDI equals sNDI for fully actuated systems, with the same number of actuators as pseudo-controls, using a pseudoinverse control allocation. For overactuated systems, both are only equal if a restoring term is applied in the INDI control allocation. The paper presents countermeasures for both methods to prevent limit cycles and instabilities resulting from linearization errors. Further, we demonstrate that the sNDI controller can be successfully applied to a skewing-wing eVTOL.

The paper is outlined as follows. In Section II, both INDI and sNDI are derived using two different approaches. Then, the equality of both structures for different system types, using simulation examples, is discussed in Section III. In the following, the effect of restoring in the control allocation is presented in Section IV and the solution using nonlinear control allocation is shown in Section V. In Section VI, we demonstrate the applicability of the sNDI algorithm on a real-world flight test of a skewing-wing uncrewed aerial vehicle (UAV). Section VII wraps up the results.

II. DERIVATION OF INCREMENTAL AND SENSORY NDI

First, the general derivation of an NDI controller is presented. The system in the NDI derivation is usually assumed to be input affine [25].

A. DERIVATION FOR INPUT-AFFINE SYSTEMS

We define an input affine multiple input multiple output (MIMO) system:

$$\dot{\boldsymbol{x}} = \boldsymbol{f}(\boldsymbol{x}) + \boldsymbol{G}(\boldsymbol{x})\boldsymbol{u} \tag{1}$$

$$\boldsymbol{y} = \boldsymbol{h}(\boldsymbol{x}), \tag{2}$$

where $\text{rank}(\boldsymbol{G}(\boldsymbol{x})) \geq n$ with n control outputs. NDI (also named feedback linearization) is based on the idea of taking

the time derivative of the output $\boldsymbol{y} = \boldsymbol{h}(\boldsymbol{x})$ until the input $\boldsymbol{u}$ appears explicitly in the equation. The derivative of the i-th output $y_i^{(r_i)} = \nu_i$ is called pseudo-control, and the number of differentiations r_i is named the relative degree [26, pp. 75-76]. The overall total relative degree is the sum of the relative degrees of all outputs. Therefore, the total relative degree is $r = r_1 + \ldots + r_n$. This system transformation can be denoted using the so-called Lie derivative [26, p. 237-238]. We define the Lie derivative of a scalar function $h_i(\boldsymbol{x})$, which is the i-th entry of $\boldsymbol{h}(\boldsymbol{x})$, along a vector field $\boldsymbol{f}(\boldsymbol{x})$ as

$$\mathcal{L}_f h_i(\boldsymbol{x}) = \mathcal{L}_f^1 h_i(\boldsymbol{x}) = \frac{\partial h_i(\boldsymbol{x})}{\partial \boldsymbol{x}} \boldsymbol{f}(\boldsymbol{x}), \tag{3}$$

where $\mathcal{L}_f^1 h_i(\boldsymbol{x})$ is the first Lie derivative [25, p. 230]. This concept is extended to higher orders as

$$\mathcal{L}_f^k h_i(\boldsymbol{x}) = \frac{\partial \mathcal{L}_f^{(k-1)} h_i(\boldsymbol{x})}{\partial \boldsymbol{x}} \boldsymbol{f}(\boldsymbol{x}), \tag{4}$$

where for $k = 0$ the Lie derivative is defined as $\mathcal{L}_f^0 h_i(\boldsymbol{x}) = h_i(\boldsymbol{x})$ [25, p. 230].

By that, the relative degree r_i of each output y_i can be found through

$$\begin{aligned} {}^{(r_i-1)}y_i &= \mathcal{L}_f^{(r_i-1)} h_i(\boldsymbol{x}) + \cancelto{0}{\frac{\partial \mathcal{L}_f^{(r_i-2)} h_i(\boldsymbol{x})}{\partial \boldsymbol{x}}} \boldsymbol{G}_i(\boldsymbol{x})\boldsymbol{u}, && (5)\\ {}^{(r_i)}y_i &= \mathcal{L}_f^{r_i} h_i(\boldsymbol{x}) + \frac{\partial \mathcal{L}_f^{(r_i-1)} h_i(\boldsymbol{x})}{\partial \boldsymbol{x}} \boldsymbol{G}_i(\boldsymbol{x})\boldsymbol{u}, && (6)\\ &= \mathcal{L}_f^{r_i} h_i(\boldsymbol{x}) + \mathcal{L}_{\boldsymbol{G}_i}^1 \mathcal{L}_f^{(r_i-1)} h_i(\boldsymbol{x})\boldsymbol{u}, && (7) \end{aligned}$$

where the vector of output derivatives is denoted as

$$\boldsymbol{\nu} = \begin{bmatrix} {}^{(r_1)}y_1 & {}^{(r_2)}y_2 & \cdots & {}^{(r_n)}y_n \end{bmatrix}^T. \tag{8}$$

Applying the transformations from (7) to each row i in (1), we arrive at

$$\boldsymbol{\nu} = \boldsymbol{f}_\nu(\boldsymbol{x}) + \boldsymbol{G}_\nu(\boldsymbol{x})\boldsymbol{u}. \tag{9}$$

Here,

$$\boldsymbol{\nu} = \begin{bmatrix} {}^{(r_1)}y_1 \\ {}^{(r_2)}y_2 \\ \vdots \\ {}^{(r_n)}y_n \end{bmatrix}, \quad \boldsymbol{f}_\nu(\boldsymbol{x}) = \begin{bmatrix} \mathcal{L}_f^{r_1} h_1(\boldsymbol{x}) \\ \mathcal{L}_f^{r_2} h_2(\boldsymbol{x}) \\ \vdots \\ \mathcal{L}_f^{r_n} h_n(\boldsymbol{x}) \end{bmatrix}, \tag{10}$$

where $\boldsymbol{f}_\nu(\boldsymbol{x}) \in \mathbb{R}^n$ contains the solely state dependent terms [25, Ch. 6.5]. Further,

$$\boldsymbol{G}_\nu(\boldsymbol{x}) = \begin{bmatrix} \mathcal{L}_{G_1}\mathcal{L}_f^{(r_1-1)} h_1(\boldsymbol{x}) & \cdots & \mathcal{L}_{G_n}\mathcal{L}_f^{(r_1-1)} h_1(\boldsymbol{x}) \\ \mathcal{L}_{G_1}\mathcal{L}_f^{(r_2-1)} h_2(\boldsymbol{x}) & \cdots & \mathcal{L}_{G_n}\mathcal{L}_f^{(r_2-1)} h_2(\boldsymbol{x}) \\ \vdots & \cdots & \vdots \\ \mathcal{L}_{G_1}\mathcal{L}_f^{(r_n-1)} h_n(\boldsymbol{x}) & \cdots & \mathcal{L}_{G_n}\mathcal{L}_f^{(r_n-1)} h_n(\boldsymbol{x}) \end{bmatrix} \tag{11}$$

where $\boldsymbol{G}_\nu(\boldsymbol{x}) \in \mathbb{R}^{n\times m}$ is named control effectiveness matrix.

Based on (9), the NDI control law of this system is obtained by solving for $\boldsymbol{u}$, resulting in

$$\boldsymbol{u}_{\text{cmd}} = \boldsymbol{G}_\nu(\boldsymbol{x})^{-1} \left(\boldsymbol{\nu}_{\text{des}} - \boldsymbol{f}_\nu(\boldsymbol{x})\right), \tag{12}$$

where the inverse $\boldsymbol{G}_\nu(\boldsymbol{x})^{-1}$ is some generalized nonlinear inverse of the matrix of functions $\boldsymbol{G}_\nu(\boldsymbol{x})$. One way to derive the sNDI law is based directly on (12), which is the one used in [21].

An alternative way to derive the control law starts from the difference between the measured pseudo-control $\boldsymbol{\nu}_0$ and the desired $\boldsymbol{\nu}_{\text{des}}$:

$$\boldsymbol{\nu}_{\text{des}} - \boldsymbol{\nu}_0 = \boldsymbol{f}_\nu(\boldsymbol{x}) - \boldsymbol{f}_\nu(\boldsymbol{x}_0) + \boldsymbol{G}_\nu(\boldsymbol{x})\boldsymbol{u} - \boldsymbol{G}_\nu(\boldsymbol{x}_0)\boldsymbol{u}_0. \tag{13}$$

Since the instant response of $\boldsymbol{u}$ is assumed, the state $\boldsymbol{x} = \boldsymbol{x}_0$ is equal to the measured one. This leads to simplification of (13), resulting in

$$\begin{aligned} \boldsymbol{\nu}_{\text{des}} - \boldsymbol{\nu}_0 = {} & \cancel{\boldsymbol{f}_\nu(\boldsymbol{x}_0) - \boldsymbol{f}_\nu(\boldsymbol{x}_0)} \\ & + \boldsymbol{G}_\nu(\boldsymbol{x}_0)\boldsymbol{u} - \boldsymbol{G}_\nu(\boldsymbol{x}_0)\boldsymbol{u}_0. \end{aligned} \tag{14}$$

To obtain the sNDI law, (14) is solved for $\boldsymbol{u}_{\text{cmd}}$. Using the Moore-Penrose pseudoinverse of the constant matrix $\boldsymbol{G}_\nu(\boldsymbol{x}_0)$, the sNDI is obtained.

$$\boldsymbol{u}_{\text{cmd}} = \boldsymbol{G}_\nu(\boldsymbol{x}_0)^+ \left[\boldsymbol{\nu}_{\text{des}} - \boldsymbol{\nu}_0 + \boldsymbol{G}_\nu(\boldsymbol{x}_0)\boldsymbol{u}_0\right]. \tag{15}$$

Based on the same (14), the INDI control law can be derived. Instead of solving for $\boldsymbol{u}_{\text{cmd}}$, one solves for the physical increment $\Delta\boldsymbol{u} = \boldsymbol{u}_{\text{cmd}} - \boldsymbol{u}_0$ first.

$$\underbrace{\boldsymbol{u}_{\text{cmd}} - \boldsymbol{u}_0}_{\Delta\boldsymbol{u}} = \boldsymbol{G}_\nu(\boldsymbol{x}_0)^+ \underbrace{(\boldsymbol{\nu}_{\text{des}} - \boldsymbol{\nu}_0)}_{\Delta\boldsymbol{\nu}}. \tag{16}$$

The last step involves transforming back to the global $\boldsymbol{u}_{\text{cmd}}$, resulting in

$$\boldsymbol{u}_{\text{cmd}} = \boldsymbol{G}_\nu(\boldsymbol{x}_0)^+ \underbrace{(\boldsymbol{\nu}_{\text{des}} - \boldsymbol{\nu}_0)}_{\Delta\boldsymbol{\nu}} + \boldsymbol{u}_0. \tag{17}$$

From now on, we will call the constant matrix $\boldsymbol{G}_\nu(\boldsymbol{x}_0) = \boldsymbol{B}$.

The sNDI law can also be derived from the NDI law directly by replacing $\boldsymbol{f}_\nu(\boldsymbol{x})$ with a measurement, also assuming $\boldsymbol{x} = \boldsymbol{x}_0$ [24].

$$\boldsymbol{f}_\nu(\boldsymbol{x}_0) = \boldsymbol{\nu}_0 - \boldsymbol{G}_\nu(\boldsymbol{x}_0)\boldsymbol{u}_0. \tag{18}$$

This then leads to

$$\boldsymbol{u}_{\text{cmd}} = \boldsymbol{G}_\nu(\boldsymbol{x}_0)^{-1} \left[\boldsymbol{\nu}_{\text{des}} - \boldsymbol{\nu}_0 + \boldsymbol{G}_\nu(\boldsymbol{x}_0)\boldsymbol{u}_0\right], \tag{19}$$

which is the sNDI law, see (15).

B. DERIVATION FOR INPUT NON-AFFINE SYSTEMS

Bacon [27] first presented the derivation for nonlinear and input non-affine systems using Taylor approximation. In this paper, a difference-based derivation is used. It starts with the following general nonlinear system.

$$\dot{\boldsymbol{x}} = \boldsymbol{f}(\boldsymbol{x}) + \boldsymbol{g}(\boldsymbol{x}, \boldsymbol{u}) = \boldsymbol{F}(\boldsymbol{x}, \boldsymbol{u}), \tag{20}$$

$$\boldsymbol{y} = \boldsymbol{h}(\boldsymbol{x}). \tag{21}$$

The system is transformed similarly to Section II-A by finding the relative degree of each output and rewriting in terms of the pseudo-control vector $\boldsymbol{\nu}$. This results in the following transformed system

$$\underbrace{\begin{bmatrix} \overset{(r_1)}{y_1} \\ \overset{(r_2)}{y_2} \\ \vdots \\ \overset{(r_n)}{y_n} \end{bmatrix}}_{\boldsymbol{\nu}} = \underbrace{\begin{bmatrix} \mathcal{L}_f^{r_1} h_1(\boldsymbol{x}) \\ \mathcal{L}_f^{r_2} h_2(\boldsymbol{x}) \\ \vdots \\ \mathcal{L}_f^{r_n} h_n(\boldsymbol{x}) \end{bmatrix}}_{\boldsymbol{f}_\nu(\boldsymbol{x})} + \underbrace{\begin{bmatrix} \mathcal{L}_{\boldsymbol{g}(\boldsymbol{x},\boldsymbol{u})} \mathcal{L}_f^{(r_1-1)} h_1(\boldsymbol{x}) \\ \mathcal{L}_{\boldsymbol{g}(\boldsymbol{x},\boldsymbol{u})} \mathcal{L}_f^{(r_2-1)} h_2(\boldsymbol{x}) \\ \vdots \\ \mathcal{L}_{\boldsymbol{g}(\boldsymbol{x},\boldsymbol{u})} \mathcal{L}_f^{(r_n-1)} h_n(\boldsymbol{x}) \end{bmatrix}}_{\boldsymbol{g}_\nu(\boldsymbol{x},\boldsymbol{u})}, \tag{22}$$

which is written short as

$$\boldsymbol{\nu} = \boldsymbol{f}_\nu(\boldsymbol{x}) + \boldsymbol{g}_\nu(\boldsymbol{x}, \boldsymbol{u}). \tag{23}$$

Similar to (13), the derivation starts with the difference between the current pseudo-control $\boldsymbol{\nu}_0$ and the desired one $\boldsymbol{\nu}_{\text{des}}$.

$$\boldsymbol{\nu}_{\text{des}} - \boldsymbol{\nu}_0 = \boldsymbol{f}_\nu(\boldsymbol{x}) - \boldsymbol{f}_\nu(\boldsymbol{x}_0) + \boldsymbol{g}_\nu(\boldsymbol{x}, \boldsymbol{u}) - \boldsymbol{g}_\nu(\boldsymbol{x}_0, \boldsymbol{u}_0). \tag{24}$$

With the assumption $\boldsymbol{x} = \boldsymbol{x}_0$, the difference simplifies as follows:

$$\begin{aligned} \boldsymbol{\nu}_{\text{des}} - \boldsymbol{\nu}_0 = {} & \cancel{\boldsymbol{f}_\nu(\boldsymbol{x}_0) - \boldsymbol{f}_\nu(\boldsymbol{x}_0)} \\ & + \boldsymbol{g}_\nu(\boldsymbol{x}_0, \boldsymbol{u}) - \boldsymbol{g}_\nu(\boldsymbol{x}_0, \boldsymbol{u}_0). \end{aligned} \tag{25}$$

Now, bringing all constant terms to the left side leads to:

$$\boldsymbol{\nu}_{\text{des}} - \boldsymbol{\nu}_0 + \boldsymbol{g}_\nu(\boldsymbol{x}_0, \boldsymbol{u}_0) = \boldsymbol{g}_\nu(\boldsymbol{x}_0, \boldsymbol{u}), \tag{26}$$

where the nonlinear vector field $\boldsymbol{g}_\nu(\boldsymbol{x}_0, \boldsymbol{u})$ can be expanded using the Taylor expansion to:

$$\begin{aligned} & \boldsymbol{\nu}_{\text{des}} - \boldsymbol{\nu}_0 + \boldsymbol{g}_\nu(\boldsymbol{x}_0, \boldsymbol{u}_0) \\ & = \boldsymbol{g}_\nu(\boldsymbol{x}_0, \boldsymbol{u}_0) + \underbrace{\left.\frac{\partial \boldsymbol{g}(\boldsymbol{x}_0, \boldsymbol{u})}{\partial \boldsymbol{u}}\right|_{\boldsymbol{u}=\boldsymbol{u}_0}}_{\boldsymbol{B}} \underbrace{(\boldsymbol{u} - \boldsymbol{u}_0)}_{\Delta \boldsymbol{u}} + \text{h.o.t.} \end{aligned} \tag{27}$$

Subtracting $\boldsymbol{g}_\nu(\boldsymbol{x}_0, \boldsymbol{u}_0)$ on both sides leads to:

$$\boldsymbol{\nu}_{\text{des}} - \boldsymbol{\nu}_0 = \boldsymbol{B}(\boldsymbol{u} - \boldsymbol{u}_0) + \text{h.o.t.}. \tag{28}$$

The higher-order terms are neglected in the following, and the final control problem can be written down as

$$\boldsymbol{\nu}_{\text{des}} - \boldsymbol{\nu}_0 = \boldsymbol{B}(\boldsymbol{u}_{\text{cmd}} - \boldsymbol{u}_0), \tag{29}$$

where $\boldsymbol{u}$ has been replaced by $\boldsymbol{u}_{\text{cmd}}$.

We can either solve for $\Delta \boldsymbol{u}$ or directly $\boldsymbol{u}_{\text{cmd}}$, which will lead to different results depending on whether $\boldsymbol{B}$ is invertible. Solving for $\boldsymbol{u}$ leads to the sNDI control law

$$\boldsymbol{B}\boldsymbol{u}_{\text{cmd}} = \boldsymbol{\nu}_{\text{des}} - \boldsymbol{\nu}_0 + \boldsymbol{B}\boldsymbol{u}_0 \tag{30}$$

$$\boldsymbol{u}_{\text{cmd}} = \boldsymbol{B}^+ (\boldsymbol{\nu}_{\text{des}} - \boldsymbol{\nu}_0 + \boldsymbol{B}\boldsymbol{u}_0) \tag{31}$$

If we first solve for $\Delta \boldsymbol{u} = \boldsymbol{u}_{\text{cmd}} - \boldsymbol{u}_0$ and then for $\boldsymbol{u}$, we arrive at the INDI control law.

$$\boldsymbol{B}(\boldsymbol{u}_{\text{cmd}} - \boldsymbol{u}_0) = \boldsymbol{\nu}_{\text{des}} - \boldsymbol{\nu}_0 \tag{32}$$

$$\boldsymbol{u}_{\text{cmd}} = \boldsymbol{B}^+ (\boldsymbol{\nu}_{\text{des}} - \boldsymbol{\nu}_0) + \boldsymbol{u}_0 \tag{33}$$

The result is that the Moore-Penrose pseudoinverse either minimizes $\boldsymbol{u}_{\text{cmd}}$ or $\Delta \boldsymbol{u}_{\text{cmd}}$ given an overactuated system. To simplify the upcoming analysis, we assume the input commands do not saturate.

The approach in [24] first replaces $\boldsymbol{f}_\nu(\boldsymbol{x})$ with a measurement and then solves for $\boldsymbol{g}_\nu(\boldsymbol{x}_0, \boldsymbol{u})$. The Taylor expansion is then applied within the nonlinear allocation problem around an arbitrary point $\boldsymbol{u}_0$ [24].

The block diagrams of the INDI and the sNDI controller are given in Figs. 1 and 2. In the following, we neglect the actuator dynamics, such that $\boldsymbol{A}(s) = \boldsymbol{I}$. Further, the measurement and filtering dynamics $\boldsymbol{H}(\boldsymbol{z})$ are neglected and modeled as a first-order unit-delay system, $\boldsymbol{H}(\boldsymbol{z}) = z^{-1}$, since the noise-free case is assumed in this paper.

C. THE MOORE-PENROSE PSEUDOINVERSE

We briefly recall the relevant rules of the Moore-Penrose pseudoinverse. One condition of the pseudoinverse is that

$$\boldsymbol{B} = \boldsymbol{B}\boldsymbol{B}^+\boldsymbol{B}. \tag{34}$$

For overactuated systems with $m > n$, where m is the number of inputs and n the number of states, the right pseudoinverse is given by

$$\boldsymbol{B}^+ = \boldsymbol{B}^T \left(\boldsymbol{B}\boldsymbol{B}^T\right)^{-1}. \tag{35}$$

From (34) and (35) it is easy to see that $\boldsymbol{B}\boldsymbol{B}^+ = \boldsymbol{I}$ but also $\boldsymbol{B}^+\boldsymbol{B} \neq \boldsymbol{I}$ if $m > n$. On the other hand, for underactuated systems with $m \leq n$, it holds that $\boldsymbol{B}^+\boldsymbol{B} = \boldsymbol{I}$, which is not considered further in this paper. In case $n = m$, the number of states is equal to the number of inputs, $\boldsymbol{B}$ is invertible, and the pseudoinverse is equal to the standard inverse such that $\boldsymbol{B}^+ = \boldsymbol{B}^{-1}$.

The Moore-Penrose pseudoinverse is used for control allocation since it is the solution to the unconstrained control allocation problem

$$\begin{aligned} \boldsymbol{u}_{\text{cmd}} = \arg\min_{\boldsymbol{u}} \ & \frac{1}{2}(\boldsymbol{u} - \boldsymbol{u}_{\text{des}})^T (\boldsymbol{u} - \boldsymbol{u}_{\text{des}}), \\ & \text{s.t. } \boldsymbol{B}\boldsymbol{u} = \boldsymbol{\nu}_{\text{des}}, \end{aligned} \tag{36}$$

where $\boldsymbol{\nu}_{\text{des}}$ is the desired pseudo-control and $\boldsymbol{u}_{\text{des}}$ is a desired control input.

A Lagrange multiplier $\boldsymbol{\lambda}$ is introduced to solve (36). The Lagrange function is then defined as

$$\mathcal{L}(\boldsymbol{u}, \boldsymbol{\lambda}) = \frac{1}{2}(\boldsymbol{u} - \boldsymbol{u}_{\text{des}})^T (\boldsymbol{u} - \boldsymbol{u}_{\text{des}}) + \boldsymbol{\lambda}(\boldsymbol{\nu}_{\text{des}} - \boldsymbol{B}\boldsymbol{u}). \tag{37}$$

To arrive at the solution, we take the derivative of (37) with respect to $\boldsymbol{u}$ and $\boldsymbol{\lambda}$.

$$\frac{\partial \mathcal{L}}{\partial \boldsymbol{u}} = \boldsymbol{u}^T - \boldsymbol{u}_{\text{des}}^T - \boldsymbol{\lambda}\boldsymbol{B} = 0, \tag{38}$$

$$\frac{\partial \mathcal{L}}{\partial \boldsymbol{\lambda}} = \boldsymbol{\nu}_{\text{des}} - \boldsymbol{B}\boldsymbol{u} = 0. \tag{39}$$

Solving (38) for $\boldsymbol{u}$, we get

$$\boldsymbol{u} = \boldsymbol{B}^T \boldsymbol{\lambda}^T + \boldsymbol{u}_{\text{des}}, \tag{40}$$

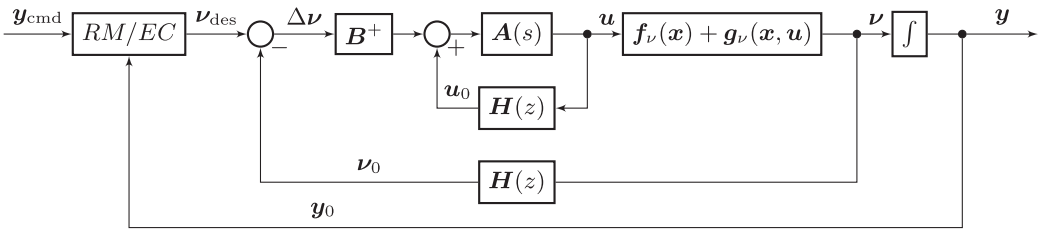

FIGURE 1. Block diagram of the standard INDI controller, where *RM/EC* represents the reference model and error controller, $A(s)$ the actuator and $H(z)$ the sensor and estimator dynamics.

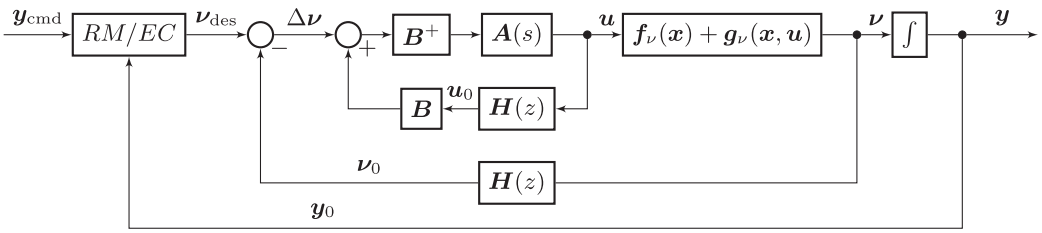

FIGURE 2. Block diagram of the sensory NDI controller, where *RM/EC* represents the reference model and error controller, $A(s)$ the actuator and $H(z)$ the sensor and estimator dynamics.

and inserting in (39) leads to

$$\boldsymbol{\nu}_{\text{des}} = \boldsymbol{B}\boldsymbol{u} = \boldsymbol{B}\boldsymbol{B}^T\boldsymbol{\lambda}^T + \boldsymbol{B}\boldsymbol{u}_{\text{des}}. \tag{41}$$

(41) is then solved for $\boldsymbol{\lambda}^T$ as

$$\boldsymbol{\lambda}^T = \left(\boldsymbol{B}\boldsymbol{B}^T\right)^{-1}\left(\boldsymbol{\nu}_{\text{des}} - \boldsymbol{B}\boldsymbol{u}_{\text{des}}\right), \tag{42}$$

which we can then re-insert into (40) leading to the solution

$$\boldsymbol{u} = \underbrace{\boldsymbol{B}^T\left(\boldsymbol{B}\boldsymbol{B}^T\right)^{-1}}_{\boldsymbol{B}^+}\left(\boldsymbol{\nu}_{\text{des}} - \boldsymbol{B}\boldsymbol{u}_{\text{des}}\right) + \boldsymbol{u}_{\text{des}}. \tag{43}$$

For a desired input $\boldsymbol{u}_{\text{des}} = \boldsymbol{0}$, the allocation simplifies to the pseudoinverse.

III. EQUALITY OF INCREMENTAL AND SENSORY NDI WITH PSEUDOINVERSE CONTROL ALLOCATION

First, we investigate whether INDI and sNDI yield equivalent control results for a pseudoinverse control allocation with desired input $\boldsymbol{u}_{\text{des}} = \boldsymbol{0}$. A pseudoinverse control allocation is used in the derivations, since the control input limits are neglected. The use of the pseudoinverse highlights the differences between incremental and global allocation, whereas in practice, incremental control allocation should always include a restoring term.

A. FULLY- AND UNDERACTUATED SYSTEMS

This is the case for all types of systems (linear, input affine, and nonlinear) if $\boldsymbol{B}$ is square and invertible (fully actuated system) or if $\boldsymbol{B}$ is a tall matrix (underactuated system). In those cases, it holds that $\boldsymbol{B}^+\boldsymbol{B} = \boldsymbol{I}$. For that, we transform (31) to

$$\begin{aligned}\boldsymbol{u}_{\text{cmd}} &= \boldsymbol{B}^+\left(\boldsymbol{\nu} - \boldsymbol{\nu}_0\right) + \boldsymbol{B}^+\boldsymbol{B}\boldsymbol{u}_0 \\ &= \boldsymbol{B}^+\left(\boldsymbol{\nu} - \boldsymbol{\nu}_0\right) + \boldsymbol{u}_0,\end{aligned} \tag{44}$$

which is then equal to the INDI law in (33). This proves the equality of INDI and sNDI under the given conditions. One should note that a desired $\boldsymbol{u}_{\text{des}} \neq \boldsymbol{0}$ will have no effect in the fully actuated system, where $\boldsymbol{B}^+ = \boldsymbol{B}^{-1}$, since

$$\begin{aligned}\boldsymbol{u} &= \boldsymbol{B}^{-1}\left(\boldsymbol{\nu}_{\text{des}} - \boldsymbol{B}\boldsymbol{u}_{\text{des}}\right) + \boldsymbol{u}_{\text{des}} \\ &= \boldsymbol{B}^{-1}\boldsymbol{\nu}_{\text{des}} - \cancel{\boldsymbol{B}^{-1}\boldsymbol{B}\boldsymbol{u}_{\text{des}}} + \cancel{\boldsymbol{u}_{\text{des}}}.\end{aligned} \tag{45}$$

For the underactuated case, a different derivation from Section II-C is required.

B. OVERACTUATED SYSTEMS

For overactuated systems, the two control approaches yield different results. Since $\boldsymbol{B}^+\boldsymbol{B} \neq \boldsymbol{I} \in \mathbb{R}^{m\times m}$, while $\boldsymbol{B}\boldsymbol{B}^+ = \boldsymbol{I} \in \mathbb{R}^{n\times n}$, the commanded input $\boldsymbol{u}_{\text{cmd}}$ is different. The reason lies in the fact that the pseudoinverse in an incremental control allocation minimizes $\|\Delta\boldsymbol{u}_{\text{cmd}}\|_2$ as in INDI, while in a global control allocation it minimizes $\|\boldsymbol{u}_{\text{cmd}}\|_2$ as in sNDI.

To evaluate if the same control performance in terms of the pseudocontrol $\boldsymbol{\nu}$ is achieved, the sNDI control law is inserted into the nonlinear plant (23) or for input affine systems (9). INDI will result in the following equation by inserting (33) into (23):

$$\begin{aligned}\boldsymbol{\nu} &= \boldsymbol{f}_\nu(\boldsymbol{x}) + \boldsymbol{g}(\boldsymbol{x}, \boldsymbol{u}_{\text{cmd}}) \\ &= \boldsymbol{f}_\nu(\boldsymbol{x}) + \boldsymbol{g}\left(\boldsymbol{x}, \boldsymbol{B}^+\left(\boldsymbol{\nu}_{\text{des}} - \boldsymbol{\nu}_0\right) + \boldsymbol{u}_0\right),\end{aligned} \tag{46}$$

whereas sNDI will result by inserting (31) into (23) in:

$$\boldsymbol{\nu} = \boldsymbol{f}_\nu(\boldsymbol{x}) + \boldsymbol{g}\left(\boldsymbol{x}, \boldsymbol{B}^+\left(\boldsymbol{\nu}_{\text{des}} - \boldsymbol{\nu}_0\right) + \boldsymbol{B}^+\boldsymbol{B}\boldsymbol{u}_0\right), \tag{47}$$

which we will evaluate for different types of systems in the following sections.

For that, simulation examples are provided, and the corresponding data can be found in [28]. The simulations are

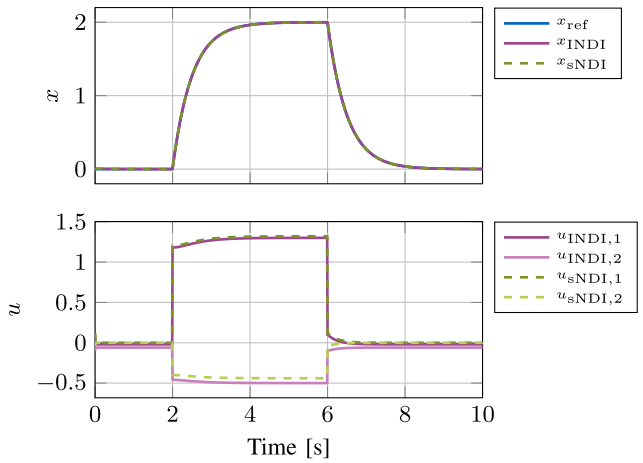

FIGURE 3. Closed loop simulation results of an input linear system for an INDI and sNDI controller.

performed in MATLAB/Simulink using the Runge-Kutta solver and a step time of 0.01 sec. The reference model used with the INDI and sNDI controller is a first order linear system with a time constant of 0.5 sec:

$$\boldsymbol{\nu}_{\text{ref}} = \dot{\boldsymbol{y}}_{\text{ref}} = 2\left(\boldsymbol{y}_{\text{cmd}} - \boldsymbol{y}_{\text{ref}}\right), \tag{48}$$

where $\boldsymbol{y}_{\text{cmd}}$ is the command input to the reference model. The error controller is a proportional controller with gain $\boldsymbol{K} = 2$, such that

$$\boldsymbol{\nu}_{\text{des}} = \boldsymbol{\nu}_{\text{ref}} + \boldsymbol{K}\left(\boldsymbol{y}_{\text{ref}} - \boldsymbol{y}\right). \tag{49}$$

1) SYSTEMS WITH LINEAR INPUT TERM

For systems linear in the input vector $\boldsymbol{u}$, we get for the sNDI from (47)

$$\begin{aligned}\boldsymbol{\nu} &= \boldsymbol{f}_{\nu}(\boldsymbol{x}) + \boldsymbol{B}\left(\boldsymbol{B}^{+}\left(\boldsymbol{\nu}_{\text{des}} - \boldsymbol{\nu}_0 + \boldsymbol{B}\boldsymbol{u}_0\right)\right)\\ &= \boldsymbol{f}_{\nu}(\boldsymbol{x}) + \left(\boldsymbol{\nu}_{\text{des}} - \boldsymbol{\nu}_0\right) + \boldsymbol{B}\boldsymbol{u}_0,\end{aligned} \tag{50}$$

where property $\boldsymbol{B}\boldsymbol{B}^{+}\boldsymbol{B} = \boldsymbol{B}$ of the pseudoinverse is used, see (34). The resulting tracking equation of the pseudo-control is identical to INDI

$$\begin{aligned}\boldsymbol{\nu} &= \boldsymbol{f}_{\nu}(\boldsymbol{x}) + \boldsymbol{B}\left(\boldsymbol{B}^{+}\left(\boldsymbol{\nu}_{\text{des}} - \boldsymbol{\nu}_0\right) + \boldsymbol{u}_0\right)\\ &= \boldsymbol{f}_{\nu}(\boldsymbol{x}) + \left(\boldsymbol{\nu}_{\text{des}} - \boldsymbol{\nu}_0\right) + \boldsymbol{B}\boldsymbol{u}_0.\end{aligned} \tag{51}$$

To demonstrate the equivalence, we provide a simulation example. The differential state equation is given as

$$\dot{v} = -(2x + 0.1x^2) + \underbrace{\begin{bmatrix}3 & -1\end{bmatrix}}_{\boldsymbol{B}}\boldsymbol{u}. \tag{52}$$

In this and the following examples, $y = x$ and $\dot{x} = v$ are assumed. As shown by the previous analysis, the pseudo-control and the state reference tracking should be equal between sNDI and INDI.

Fig. 3 illustrates the state tracking and allocated inputs for both methods using a step input.Both methods track the reference signal perfectly, while the used inputs vary. The CA in sNDI drives the inputs to zero for a zero reference signal, while INDI converges to a trim input off the zero vector. This demonstrates that sNDI truly minimizes the input vector, whereas INDI minimizes the increments when pseudoinverse control allocation is used.

2) NONLINEAR INPUT AFFINE SYSTEMS

For nonlinear but input affine systems, it can again be proven that INDI and sNDI will result in identical pseudo-control tracking even though the inputs differ. As a first step, we use the input affine system (1) and the corresponding sNDI law (15).

$$\begin{aligned}\boldsymbol{\nu} &= \boldsymbol{f}_{\nu}(\boldsymbol{x}) + \boldsymbol{G}_{\nu}(\boldsymbol{x})\left(\boldsymbol{B}^{+}\left(\boldsymbol{\nu}_{\text{des}} - \boldsymbol{\nu}_0 + \boldsymbol{B}\boldsymbol{u}_0\right)\right)\\ &= \boldsymbol{f}_{\nu}(\boldsymbol{x}) + \boldsymbol{G}_{\nu}(\boldsymbol{x})\boldsymbol{B}^{+}\left(\boldsymbol{\nu}_{\text{des}} - \boldsymbol{\nu}_0\right)\\ &\quad + \boldsymbol{G}_{\nu}(\boldsymbol{x})\boldsymbol{B}^{+}\boldsymbol{B}\boldsymbol{u}_0,\end{aligned} \tag{53}$$

where $\boldsymbol{B} = \boldsymbol{G}_{\nu}(\boldsymbol{x}_0)$. Assuming exact model knowledge of $\boldsymbol{G}_{\nu}(\boldsymbol{x})$ and $\boldsymbol{x} = \boldsymbol{x}_0$, we get

$$\boldsymbol{G}_{\nu}(\boldsymbol{x}_0)\boldsymbol{B}^{+}\boldsymbol{B} = \boldsymbol{B}\boldsymbol{B}^{+}\boldsymbol{B} = \boldsymbol{B}. \tag{54}$$

(53) is then equal to the INDI pseudo-control equation

$$\begin{aligned}\boldsymbol{\nu} &= \boldsymbol{f}_{\nu}(\boldsymbol{x}) + \boldsymbol{G}_{\nu}(\boldsymbol{x})\left(\boldsymbol{B}^{+}\left(\boldsymbol{\nu}_{\text{des}} - \boldsymbol{\nu}_0\right) + \boldsymbol{u}_0\right)\\ &= \boldsymbol{f}_{\nu}(\boldsymbol{x}) + \left(\boldsymbol{\nu}_{\text{des}} - \boldsymbol{\nu}_0\right) + \boldsymbol{B}\boldsymbol{u}_0,\end{aligned} \tag{55}$$

where again $\boldsymbol{x} = \boldsymbol{x}_0$ is assumed.

As an example, the following input affine state space system has been chosen

$$\dot{v} = -(2x + 0.1x^2) + \underbrace{3u_1 - x^2 \cdot u_2}_{\boldsymbol{G}_{\nu}(x)\boldsymbol{u}}, \tag{56}$$

where nonlinearities are only present in the state x. The resulting control effectiveness matrix is equal to

$$\boldsymbol{B} = \boldsymbol{G}_{\nu}(\boldsymbol{x}_0) = \begin{bmatrix}3 & -x_0^2\end{bmatrix}, \tag{57}$$

and is dependent on the measured state x_0.

Fig. 4 demonstrates that, as expected, the state tracking of INDI and sNDI is identical, whereas again the allocated inputs vary. The Euclidean length of the input vector of sNDI is shorter than for INDI.

3) GENERAL NONLINEAR SYSTEMS

Equality cannot be generally shown for general nonlinear systems with nonlinearities in the inputs as in (20). (46) and (47) just differ through the term $\boldsymbol{B}^{+}\boldsymbol{B}$ in front of $\boldsymbol{u}_0$. This projection moves the input vector along the tangential vector of the nonlinear function $\boldsymbol{g}(x, \boldsymbol{u})$ such that $\boldsymbol{\nu}$ stays constant as long as the linearization $\boldsymbol{B} = \frac{\partial g(x_0, \boldsymbol{u})}{\partial \boldsymbol{u}}|_{\boldsymbol{u}=\boldsymbol{u}_0}$ is valid, see (27). If the computed projection leaves this range, the linearization is no longer valid and could drive the control law unstable or into a limit cycle when

$$\boldsymbol{g}\left(\boldsymbol{x}, \boldsymbol{B}^{+}\boldsymbol{B}\boldsymbol{u}_0\right) \not\approx \boldsymbol{g}\left(\boldsymbol{x}, \boldsymbol{u}_0\right). \tag{58}$$

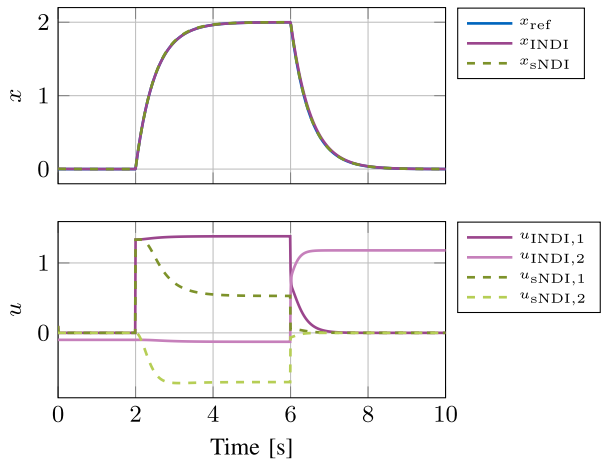

FIGURE 4. Closed loop simulation results of a nonlinear input affine system for an INDI and sNDI controller.

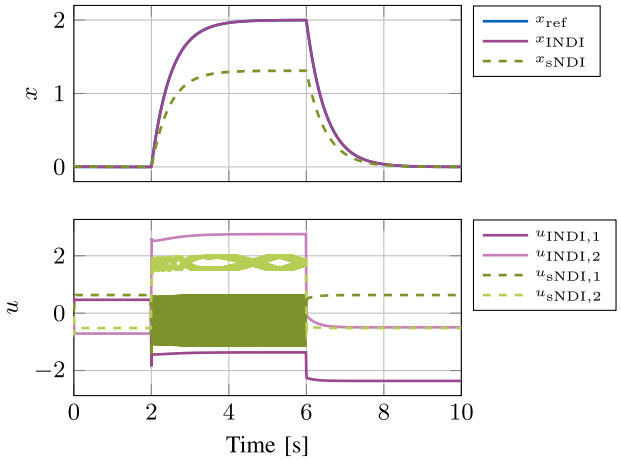

FIGURE 5. Closed loop simulation results of a nonlinear system for an INDI and sNDI controller.

With the fully nonlinear system, limit-cycles or instability can arise using the sNDI controller due to the linearization error and the allocation of the complete $\boldsymbol{u}$. To demonstrate such a case, the following nonlinear system is studied:

$$\nu = -(2x + 0.1x^2) + \underbrace{\cos(u_1) - 0.5u_1 + 0.1u_2^2 + u_2}_{g(x,\boldsymbol{u})}. \quad (59)$$

The system is nonlinear and not input affine, and the control effectiveness matrix is obtained using the Taylor approximation:

$$\boldsymbol{B} = \left.\frac{\partial g(x_0, \boldsymbol{u})}{\partial \boldsymbol{u}}\right|_{\boldsymbol{u}=\boldsymbol{u}_0} = \begin{bmatrix} -\sin(u_{1,0}) - 0.5 & 0.2u_{2,0} + 1 \end{bmatrix}. \quad (60)$$

Again, a step input is applied to both closed loops, with the results shown in Fig. 5. In Fig. 5, it can be observed that the INDI controller tracks the reference, while the sNDI controller does not. The input commands of sNDI end up in a limit cycle, jumping from ≈ -1 to ≈ 0.5 in u_1 and ≈ 1.7 to ≈ 2 in u_2. The reason for that is the allocation on the global $\boldsymbol{u}$ using the linearization $\boldsymbol{B}$. To illustrate that, the contour lines of $g(x, \boldsymbol{u})$ have been plotted together with the two terms of $\boldsymbol{u}_{\text{cmd}}$, $\boldsymbol{B}^+(\nu_{\text{des}} - \nu_0)$ and $\boldsymbol{B}^+\boldsymbol{B}\boldsymbol{u}_0$, in Fig. 6. The plotted time frame spans from 0 s to 3 s. We observe how the system begins and then, after executing the step command, enters a limit cycle. The term $\boldsymbol{B}^+\boldsymbol{B}\boldsymbol{u}_0$ first projects the commanded input towards the closest point to the origin along the tangent of the function $g(x, \boldsymbol{u})$. It can be observed that this projection leaves the validity of the linearization. Then, the input from $\boldsymbol{B}^+(\nu_{\text{des}} - \nu_0)$ is added. In the case of the limit cycle, the resulting state derivative is identical to the measured value, despite a significant increment being desired.

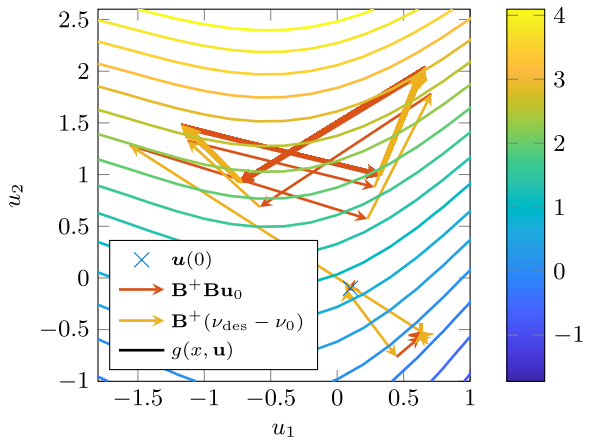

FIGURE 6. Contour plot of the nonlinear input term and the commanded input trajectory of the sNDI control law from Fig. 5 for the range of 0 s to 3 s, where the input is split in the two terms from (47), where $\mathbf{B}^+(\nu_{des} - \nu_0)$ is plotted first, followed by $\mathbf{B}^+\mathbf{B}\boldsymbol{u}_0$.

C. SUMMARY

The results of the earlier analyses can be summarized below in Table 1.

IV. EQUALITY OF INCREMENTAL AND SENSORY NDI WITH NULL-SPACE TRANSITION

In INDI, the simple pseudoinverse CA minimizes $\|\Delta\boldsymbol{u}\|$, whereas in sNDI $\|\boldsymbol{u}\|$ is minimized. This leads to a phenomenon similar to the path dependency problem [13], which we also observed in the example of Section III-B1.

The following equation illustrates the path dependency problem. The input vector $\boldsymbol{u}$ at step n can be computed as

$$\boldsymbol{u}(n) = \sum_{i=0}^{n} \Delta\boldsymbol{u}(i) = \sum_{i=0}^{n} \boldsymbol{P}\Delta\boldsymbol{\nu}(i) = \boldsymbol{P}\sum_{i=0}^{n} \Delta\boldsymbol{\nu}(i) = \boldsymbol{P}\boldsymbol{\nu}(n). \quad (61)$$

where $\boldsymbol{B}$ is a constant control effectiveness matrix, $\boldsymbol{P}$ is therefore a constant generalized inverse of $\boldsymbol{B}$, $\Delta\boldsymbol{u}$ is the input increment vector, and $\Delta\boldsymbol{\nu}(i)$ is the desired pseudo-control vector (increment) [13]. If $\boldsymbol{P}$ is constant, there is no path

TABLE 1. Overview of Equality of Incremental (INDI) and Sensory Nonlinear Dynamic Inversion (sNDI).

system type	linear	input affine	nonlinear
$m > n$	$\boldsymbol{\nu}_{\text{INDI}} = \boldsymbol{\nu}_{\text{sNDI}}$ $\boldsymbol{u}_{\text{INDI}} \neq \boldsymbol{u}_{\text{sNDI}}$	$\boldsymbol{\nu}_{\text{INDI}} = \boldsymbol{\nu}_{\text{sNDI}}$ if $\boldsymbol{x} = \boldsymbol{x}_0$ $\boldsymbol{u}_{\text{INDI}} \neq \boldsymbol{u}_{\text{sNDI}}$	$\boldsymbol{\nu}_{\text{INDI}} \neq \boldsymbol{\nu}_{\text{sNDI}}$ $\boldsymbol{u}_{\text{INDI}} \neq \boldsymbol{u}_{\text{sNDI}}$
$m = n$	$\boldsymbol{\nu}_{\text{INDI}} = \boldsymbol{\nu}_{\text{sNDI}}$ $\boldsymbol{u}_{\text{INDI}} = \boldsymbol{u}_{\text{sNDI}}$	$\boldsymbol{\nu}_{\text{INDI}} = \boldsymbol{\nu}_{\text{sNDI}}$ $\boldsymbol{u}_{\text{INDI}} = \boldsymbol{u}_{\text{sNDI}}$	$\boldsymbol{\nu}_{\text{INDI}} = \boldsymbol{\nu}_{\text{sNDI}}$ $\boldsymbol{u}_{\text{INDI}} = \boldsymbol{u}_{\text{sNDI}}$

dependency problem. In case the generalized inverse $\boldsymbol{P}(i)$ changes over time, (61) does not hold. Therefore, the final $\boldsymbol{u}(n)$ may differ depending on the allocation level (global or incremental). $\boldsymbol{P}(i)$ can change over time if $\boldsymbol{B}(i)$ changes or if $\boldsymbol{P}$ is not the same typ of generalized inverse. Therefore, the incremental allocation can lead to path dependent solutions.

A. ADDING A NULL-SPACE TRANSITION TO THE CONTROL ALLOCATION IN INDI

To overcome the path dependency problem, a restoring mechanism [29], [30], also called null-space transition [15], can be applied. This approach moves the allocated results within the null-space of the control effectiveness such that $\|\boldsymbol{u} - \boldsymbol{u}_{\text{des}}\|_2$ is minimized. Without loss of generality, we consider an actuation system without limits such that the optimum is always found directly through this one-shot approach.

We recall the CA (31) of sNDI:

$$\begin{aligned}\boldsymbol{u}_{\text{cmd}} &= \boldsymbol{B}^{+}\boldsymbol{\nu}_{\text{des}} = \boldsymbol{B}^{+}(\Delta\boldsymbol{\nu} + \boldsymbol{B}\boldsymbol{u}_0)\\ &= \boldsymbol{B}^{+}\Delta\boldsymbol{\nu} + \boldsymbol{B}^{+}\boldsymbol{B}\boldsymbol{u}_0 \end{aligned} \tag{62}$$

To integrate the restoring into the INDI (33), we use the formula for control allocation with restoring from (43). First, the global input $\boldsymbol{u}$, the global desired input $\boldsymbol{u}_{\text{des}}$, and the global desired pseudo-control $\boldsymbol{\nu}_{\text{des}}$ in (43) are replaced with their incremental counterparts leading to

$$\Delta\boldsymbol{u}_{\text{cmd}} = \boldsymbol{B}^{+}\left(\Delta\boldsymbol{\nu}_{\text{des}} - \boldsymbol{B}\Delta\boldsymbol{u}_{\text{des}}\right) + \Delta\boldsymbol{u}_{\text{des}}, \tag{63}$$

where $\Delta\boldsymbol{u}_{\text{des}} = \boldsymbol{u}_{\text{des}} - \boldsymbol{u}_0$ is the desired input increment and $\Delta\boldsymbol{\nu}_{\text{des}} = \boldsymbol{\nu}_{\text{des}} - \boldsymbol{\nu}_0$ is the desired pseudo-control increment. To obtain the control input command, the current input $\boldsymbol{u}_0$ is added as in (33), which leads to the final law

$$\begin{aligned}\boldsymbol{u}_{\text{cmd}} &= \Delta\boldsymbol{u}_{\text{cmd}} + \boldsymbol{u}_0\\ &= \boldsymbol{B}^{+}\left(\Delta\boldsymbol{\nu}_{\text{des}} - \boldsymbol{B}\Delta\boldsymbol{u}_{\text{des}}\right) + \Delta\boldsymbol{u}_{\text{des}} + \boldsymbol{u}_0, \end{aligned} \tag{64}$$

To match the cost function of the sNDI with pseudoinverse control allocation, the global desired input is $\boldsymbol{u}_{\text{des}} = \boldsymbol{0}$ Thus $\Delta\boldsymbol{u}_{\text{des}} = -\boldsymbol{u}_0$ and we arrive at

$$\begin{aligned}\boldsymbol{u}_{\text{cmd}} &= \boldsymbol{B}^{+}\left(\Delta\boldsymbol{\nu}_{\text{des}} - \boldsymbol{B}\Delta\boldsymbol{u}_{\text{des}}\right) + \Delta\boldsymbol{u}_{\text{des}} + \boldsymbol{u}_0\\ &= \boldsymbol{B}^{+}\Delta\boldsymbol{\nu}_{\text{des}} - \boldsymbol{B}^{+}\boldsymbol{B}\Delta\boldsymbol{u}_{\text{des}} + \Delta\boldsymbol{u}_{\text{des}} + \boldsymbol{u}_0\\ &= \boldsymbol{B}^{+}\Delta\boldsymbol{\nu}_{\text{des}} + \boldsymbol{B}^{+}\boldsymbol{B}\boldsymbol{u}_0 - \boldsymbol{u}_0 + \boldsymbol{u}_0\\ &= \boldsymbol{B}^{+}\Delta\boldsymbol{\nu} + \boldsymbol{B}^{+}\boldsymbol{B}\boldsymbol{u}_0, \end{aligned} \tag{65}$$

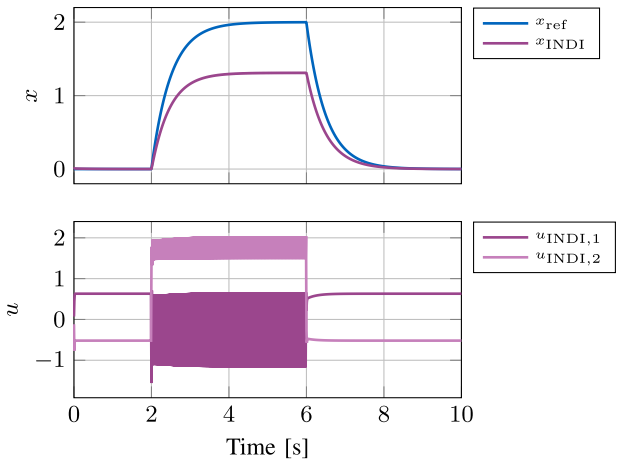

FIGURE 7. Closed loop simulation results of a nonlinear system for an INDI with null-space transition controller.

which is the same CA law as for sNDI, see (62). In the literature [29], [30], the restoring is achieved by adding a projection onto the null-space $\aleph\aleph^T = \boldsymbol{I} - \boldsymbol{B}^{+}\boldsymbol{B}$ to the pseudoinverse-based allocation. It can be shown that this is equivalent to (43), which is added in the appendix. The same also holds if both the INDI and sNDI control allocation integrate a desired input $\boldsymbol{u}_{\text{des}} \neq \boldsymbol{0}$, see Appendix for a detailed derivation.

The comparison of the CA of sNDI and INDI with null-space transition leads to the following conclusions:

- sNDI and INDI with null-space transition have the same behavior in terms of input minimization and linearization error.
- The deviation of the allocated input from $\boldsymbol{u}_0$ must be limited to the range of validity of the linearization.

For general $\boldsymbol{u}_{\text{des}}$, both approaches are also equal, as shown in the Appendix. Suppose a quadratic programming approach is used for a constrained CA problem. In that case, identical results can be expected since it finds the optimum given the same primary and secondary objectives and constraints.

B. GENERAL NONLINEAR SYSTEMS FOR INDI WITH NULL-SPACE TRANSITION

As discussed before, the minimization objective in INDI can be altered to $\|\boldsymbol{u}\|_2$ by adding a restoring/null-space transition term. To illustrate the equivalence, the nonlinear example system (59) was used with the INDI and null-space transition CA law (64). The simulation outcomes are plotted in Fig. 7. It can be seen that with the null-space transition, INDI exhibits the

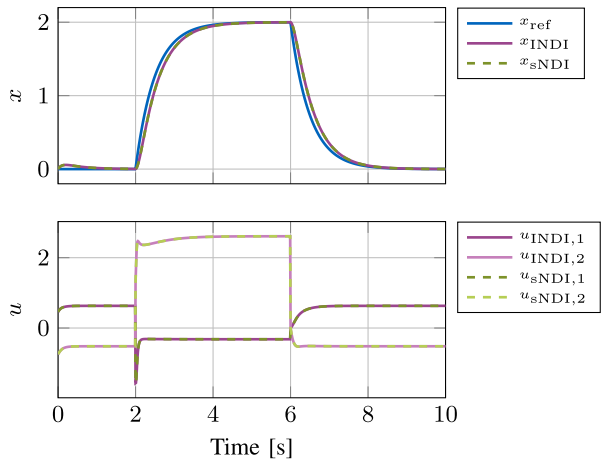

FIGURE 8. Closed loop simulation results of a nonlinear system for an INDI with null-space transition and sNDI controller with actuator in the loop.

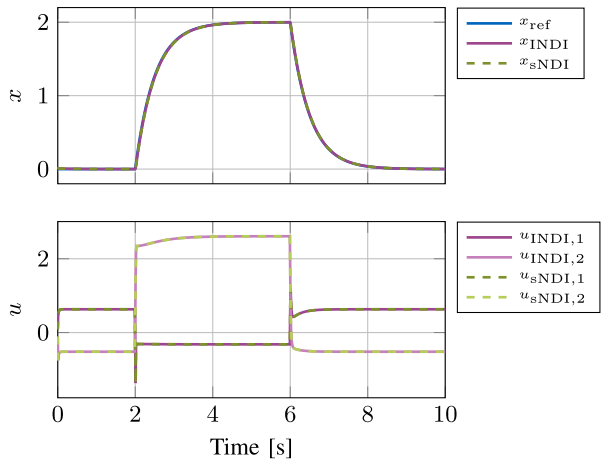

FIGURE 9. Closed loop simulation results of a nonlinear system for an INDI with null-space transition and sNDI controller with rate limits in the control allocation.

same limit cycle as sNDI. The contour plot would be similar to the one of sNDI with the difference that first $\boldsymbol{B}^{+}(\nu_{\text{des}} - \nu_0)$ is applied and then $\boldsymbol{B}^{+}\boldsymbol{B}\boldsymbol{u}_0$.

Durham observed a similar chattering phenomenon and Bordignon [13, Ch. 4.4.3] for a drag curve as a secondary objective, which is of a different origin compared to here. The reason for chattering is the significant difference from the original point. They suggest filtering the commands as a remedy [13, Ch. 4.4.3], a suggestion we also make in the following section.

C. MEASURES TO AVOID INSTABILITIES

To avoid the undesirable behavior seen in Figs. 5 and 7 for both INDI with null-space transition and sNDI, we discuss countermeasures. The provided list is surely non-exhaustive and should give suggestions to the reader. However, the primary goal is to minimize the discrepancy between the current and previous inputs acting on the system, thereby reducing large linearization errors.

Inherently, in most real systems, the actuator dynamics avoid instantaneous changes between the commanded and actual system inputs as they act as low-pass filters. In the concrete example, this avoids the limit cycle as the input u_1 does not change the sign compared to the desired input vector $\boldsymbol{u}_{\text{des}} = \boldsymbol{0}$ within one step.

To demonstrate the effect, the example from (59) was chosen using INDI with null-space transition and sNDI. First-order actuator dynamics with the following transfer function were added according to Figs. 1 and 2.

$$A(s) = \frac{10}{s + 10}. \tag{66}$$

The simulation results are presented in Fig. 8. It can be observed that the limit cycle oscillation is resolved, at the cost of a small dynamic tracking error of x_{ref}.

An alternative method can be applied to restrict the rate of change of $\boldsymbol{u}$ towards the desired input $\boldsymbol{u}_{\text{des}}$. Instead of moving the allocated input as close as possible to the desired input $\boldsymbol{u}_{\text{des}}$, the objective of the null-space transition is changed to a point between the current input $\boldsymbol{u}_0$ and the desired input, see Appendix. Note that in the example presented here $\boldsymbol{u}_{\text{des}} = \boldsymbol{0}$.

$$\boldsymbol{u}_{\text{des,sNDI}} = \boldsymbol{u}_0 + k(\boldsymbol{u}_{\text{des}} - \boldsymbol{u}_0), \tag{67}$$

$$\Delta\boldsymbol{u}_{\text{des,INDI}} = k(\boldsymbol{u}_{\text{des}} - \boldsymbol{u}_0), \tag{68}$$

where $k \in [0, 1]$ is the null-space transition gain. Through this modification, the control allocation moves the allocated input more slowly towards the desired input vector, avoiding significant linearization error.

Again, the example from (59) with INDI with null-space transition and sNDI is used to show the effect of the measure. The modified desired input (67) was incorporated into the control allocation, with k set to 0.5. The simulation results are given in Fig. 9. The effect is identical for INDI and sNDI in x_{ref} and $\boldsymbol{u}$. The optimal input configuration is reached more slowly than the non-modified version. However, no cycling behavior is triggered.

V. NONLINEAR CONTROL ALLOCATION

An alternative solution to the linear methods from before is solving the control allocation problem nonlinearly. Given a general nonlinear transformed system from (23)

$$\boldsymbol{\nu} = \boldsymbol{f}_{\nu}(\boldsymbol{x}) + \boldsymbol{g}_{\nu}(\boldsymbol{x}, \boldsymbol{u}) \tag{69}$$

one can write the difference between the desired pseudocontrol and the measured as, identical to (24), see (26),

$$\boldsymbol{\nu}_{\text{des}} - \boldsymbol{\nu}_0 = \boldsymbol{g}(\boldsymbol{x}, \boldsymbol{u}_{\text{cmd}}) - \boldsymbol{g}(\boldsymbol{x}_0, \boldsymbol{u}_0). \tag{70}$$

(70) is then solved for $\boldsymbol{u}_{\text{cmd}}$. We will note this nonlinear inversion as $\boldsymbol{g}^{-1}(\boldsymbol{x}, \boldsymbol{\nu})$, where sometimes it can be handy to

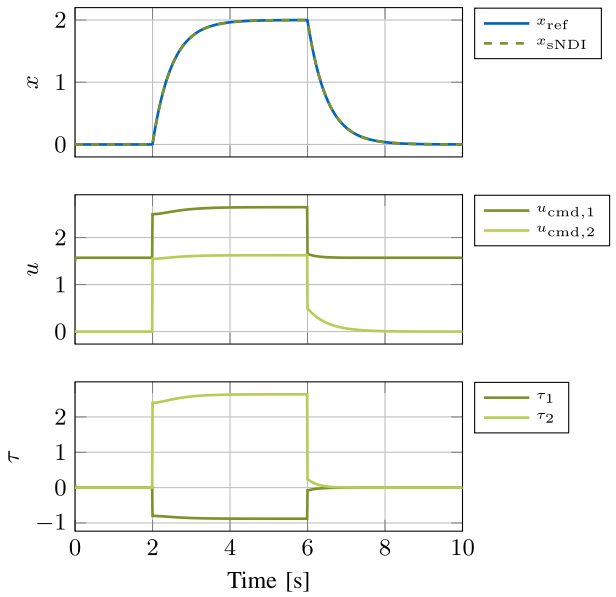

FIGURE 10. Closed loop simulation of the separable system using the nonlinear transformation.

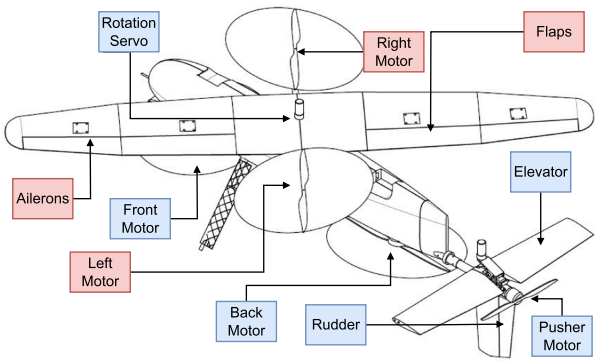

FIGURE 11. Schematic drawing of the Variable Skew Quad Plane. In red, the actuators that rotate with the wingbox.

simplify by assuming $\boldsymbol{x} = \boldsymbol{x}_0$.

$$\boldsymbol{u}_{\text{cmd}} = \boldsymbol{g}^{-1}\left(\boldsymbol{x},\, \boldsymbol{v}_{\text{des}} - \boldsymbol{v}_0 + \boldsymbol{g}(\boldsymbol{x}_0, \boldsymbol{u}_0)\right). \tag{71}$$

Transforming this nonlinear sNDI formulation into an INDI style is not possible since

$$\boldsymbol{g}^{-1}\left(\boldsymbol{x},\, \Delta\boldsymbol{v} + \boldsymbol{g}(\boldsymbol{x}_0, \boldsymbol{u}_0)\right) \neq \boldsymbol{g}^{-1}\left(\boldsymbol{x}, \Delta\boldsymbol{v}\right) + \boldsymbol{g}^{-1}\left(\boldsymbol{x}, \boldsymbol{g}(\boldsymbol{x}_0, \boldsymbol{u}_0)\right). \tag{72}$$

The nonlinear sNDI approach has been successfully applied by [22].

A commonly used alternative to full nonlinear control allocation is to separate the underdetermined allocation problem from the nonlinear inversion. This is possible for a vast group of real systems. Assuming a transformed system based on Section II-A of the following structure

$$\boldsymbol{v} = \boldsymbol{f}_v(\boldsymbol{x}) + \boldsymbol{g}(\boldsymbol{x}, \boldsymbol{u}) = \boldsymbol{f}_v(\boldsymbol{x}) + \boldsymbol{G}_\tau(\boldsymbol{x})\boldsymbol{g}_u(\boldsymbol{u}), \tag{73}$$

where $\boldsymbol{G}_\tau(\boldsymbol{x}) \in \mathbb{R}^{n\times m}$ and $\boldsymbol{g}_u(\boldsymbol{u}) \in \mathbb{R}^m \to \mathbb{R}^m$. We can now introduce the virtual control variable $\boldsymbol{\tau} = \boldsymbol{g}_u(\boldsymbol{u})$. If this is now bijective and invertible in the permissible input range, the rules of the input affine system apply.

$$\boldsymbol{v} = \boldsymbol{f}_v(\boldsymbol{x}) + \boldsymbol{G}_\tau(\boldsymbol{x})\boldsymbol{\tau} \tag{74}$$

One should note that the permutation of the new virtual inputs also alters the optimization objective of the pseudoinverse, and the box constraint limits of the real inputs can be changed to more complex constraints.

Typical examples are propellers where $\boldsymbol{g}(\boldsymbol{x}, \boldsymbol{u}) \propto \omega^2$, where ω is the propeller speed, or tilt propellers where $\boldsymbol{g}(\boldsymbol{x}, \boldsymbol{u}) \propto \begin{bmatrix} \sin(\theta)\omega^2 \\ \cos(\theta)\omega^2 \end{bmatrix}$, where θ is the tilt angle. The resulting controller would then take the form of

$$\begin{aligned} \boldsymbol{u}_{\text{cmd}} &= \boldsymbol{g}_u^{-1}(\boldsymbol{\tau}_{\text{cmd}}) \\ &= \boldsymbol{g}_u^{-1}\left(\boldsymbol{G}_\tau(\boldsymbol{x}_0)^+ \left(\Delta\boldsymbol{v} + \boldsymbol{G}_\tau(\boldsymbol{x}_0)\boldsymbol{g}_u(\boldsymbol{u}_0)\right)\right), \end{aligned} \tag{75}$$

where $\Delta\boldsymbol{v} = \boldsymbol{v}_{\text{des}} - \boldsymbol{v}_0$.

To demonstrate this approach, a simple example system was selected, given in (76).

$$\nu = -(2x + 0.1x^2) \underbrace{-0.5\cos(u_1) + 1.5u_2^2}_{\boldsymbol{G}_\tau(x)\boldsymbol{g}_u(\boldsymbol{u})} \tag{76}$$

For this system, the virtual inputs $\boldsymbol{\tau}$ and their inversion are defined as follows

$$\boldsymbol{g}_u(\boldsymbol{u}) = \begin{bmatrix} \tau_1 \\ \tau_2 \end{bmatrix} = \begin{bmatrix} \cos(u_1) \\ u_2^2 \end{bmatrix}, \tag{77}$$

$$\boldsymbol{g}_u(\boldsymbol{\tau})^{-1} = \begin{bmatrix} \arccos(u_{v,1}) \\ \sqrt{u_{v,2}} \end{bmatrix}. \tag{78}$$

The resulting state dependent matrix $\boldsymbol{G}_\tau$ simplifies to

$$\boldsymbol{G}_\tau = \begin{bmatrix} -0.5 & 1.5 \end{bmatrix}. \tag{79}$$

Although the original inputs are unlimited, the virtual ones are limited due to the nonlinear transformation. It must hold that $-1 \leq u_{v,1} \leq 1$ and $u_{v,2} \geq 0$.

Fig. 10 shows the closed-loop simulation results of the separation approach presented in (76)-(79) for a step input. The reference command is tracked well by the controlled system. The control allocation is performed on the virtual inputs $\boldsymbol{\tau}$ consisting of a pseudoinverse followed by a saturation to respect the input limits. After the backward step ($t \geq 6s$), both the virtual and actual inputs converge to the initial value from $t \leq 2s$. Since the pseudoinverse is applied to the virtual inputs only those are minimized, leading to the effect that the actual inputs are not at their minimum norm configuration ($\tau_1 = \sqrt{1/3}$ and $\tau_2 = 0$).

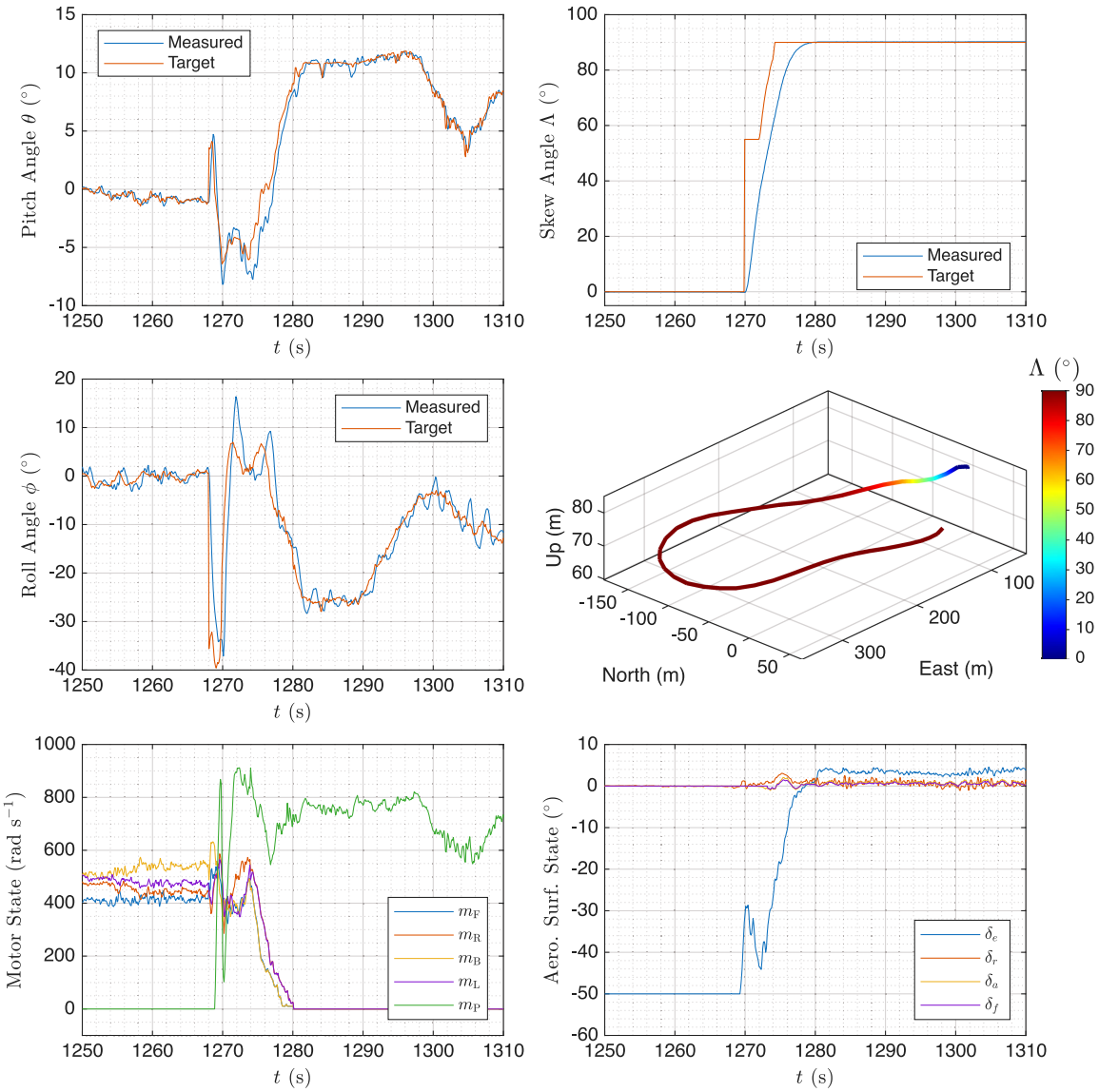

FIGURE 12. **Flight test of the sensory Nonlinear Dynamic Inversion control law using a Variable Skew Quad Plane.**

VI. EXAMPLE ON VARIABLE SKEW QUAD PLANE

This section demonstrates that the sNDI structure can be used to control a complex vehicle, in particular the Variable Skew Quad Plane (VSQP), which was previously controlled by an INDI law [31].

The VSQP, described in detail in [5] and [31], is a quadplane that utilizes variable geometry to achieve both efficient forward flight and aggressive, precise vertical flight. Its unique feature is a rotating wingbox structure that supports two lateral motors and the main wing. By rotating the wingbox 90 ° (rotation angle denoted by Λ), the drone can switch between prioritizing vertical flight performance—by stowing the wing atop the fuselage—or enabling efficient cruise flight, harnessing the lift generated by the wing. Fig. 11 illustrates the actuators available on the VSQP.

In [31], control and mode transition of the VSQP were achieved using an INDI controller, with the control law of (33), combined with a WLS control allocation scheme. The study demonstrated that, by scheduling actuator effectiveness as a function of the skew angle, the vehicle could transition autonomously from vertical flight to forward flight while maintaining the desired position setpoint.

The validation of the same controller structure of [31] but with the sNDI control law of (31) on this platform is particularly compelling because the drone must be continuously controlled across three distinct flight phases: (1) in vertical flight, stability is achieved primarily through the lifting motors; (2) in cruise flight, the VSQP behaves as a conventional fixed-wing aircraft, relying on aerodynamic control surfaces for stabilization; and (3) during the transition between these modes, the full set of actuators is blended to maintain stability.

Some key variables recorded during a transition test flight of the VSQP are shown in Fig. 12. Specifically, the figure

reports the roll angle ϕ and pitch angle θ (defined in the ZYX Euler convention), the motor states of the front, right, back, left, and pusher motors (m_F, m_R, m_B, m_L, and m_P), the deflections of the elevator, rudder, ailerons, and flaperons (δ_e, δ_r, δ_a, and δ_f), and the three-dimensional vehicle position, color-coded by the skew angle Λ. The full dataset is available through [28]. In this flight, the drone initially performed vertical flight in quad mode, ascending to gain altitude. It then accelerated forward using the pusher motor and transitioned to cruise forward flight, where it continued to fly in circles. The plots focus on the transition and demonstrate that the drone was able to closely track its attitude reference signals.

The data clearly show that during the vertical flight phase (up until approximately 1270 s), stabilization is primarily achieved using the motors. In the subsequent forward flight phase (from 1280 [s] onward), the aerodynamic surfaces are utilized for stabilization. Notably, during the transition phase (1270 to 1280 [s]), as the drone throttles down the motors and shifts to wing-generated lift, it remains overactuated and actively employs the complete set of actuators to maintain stability. The elevator of the VSQP is an all-moving control surface capable of large deflections in vertical flight (up to 50°) to reduce interference with the rear motor. During the transition phase to forward flight, its deflection is gradually reduced toward 0°.

This test flight validates the effectiveness of sNDI in both overactuated and non-overactuated scenarios, demonstrating its suitability for real-world applications during flight tests.

VII. CONCLUSION

In this paper, INDI and sNDI are compared for different classes of systems, and the applicability of sNDI to a VSQP UAV is shown. The paper demonstrates that INDI and sNDI yield identical control inputs for systems with the same number of inputs and control variables, and therefore are equivalent for those systems. For overactuated systems with more inputs than control variables, both control methods yield different commanded input vectors, resulting in a deviation in reference pseudo-control tracking.

The sNDI approach mitigates the need for restoring the inputs to their zero values but can lead to limit-cycles or even instability for specific nonlinear systems. But when restoring is applied to INDI, which is usually necessary, the allocated inputs are equal to the ones from sNDI. As a result, the same issue arises, which originates from the larger linearization error due to the offset from the linearization point by the restoring term. But the issues can be avoided by limiting the offset of the restoring term directly in the allocation or through the actuator dynamics. Since most real systems contain actuators with sufficiently slow dynamics, sNDI can be successfully applied as demonstrated with the VSQP UAV. Determining the maximum allowed increment allocated from the measured input vector to ensure validity within the linearization remains as future work.

APPENDIX

First, the equality of the null-space projection using $(\boldsymbol{I} - \boldsymbol{B}^+\boldsymbol{B})$ to (43) is shown:

$$\begin{aligned}\Delta\boldsymbol{u}_{\text{cmd}} &= \boldsymbol{B}^+\Delta\boldsymbol{\nu}_{\text{des}} \\ &\quad + (\boldsymbol{I} - \boldsymbol{B}^+\boldsymbol{B})\left(\Delta\boldsymbol{u}_{\text{des}} - \boldsymbol{B}^+\Delta\boldsymbol{\nu}_{\text{des}}\right) \\ &= \cancel{\boldsymbol{B}^+\Delta\boldsymbol{\nu}_{\text{des}}} + \Delta\boldsymbol{u}_{\text{des}} - \boldsymbol{B}^+\boldsymbol{B}\Delta\boldsymbol{u}_{\text{des}} \\ &\quad - \cancel{\boldsymbol{B}^+\Delta\boldsymbol{\nu}_{\text{des}}} + \boldsymbol{B}^+\boldsymbol{B}\boldsymbol{B}^+\Delta\boldsymbol{\nu}_{\text{des}} \\ &= \boldsymbol{B}^+\left(\Delta\boldsymbol{\nu}_{\text{des}} - \boldsymbol{B}\Delta\boldsymbol{u}_{\text{des}}\right) + \Delta\boldsymbol{u}_{\text{des}}, \end{aligned} \tag{80}$$

where the general property of the pseudoinverse $\boldsymbol{B}^+\boldsymbol{B}\boldsymbol{B}^+ = \boldsymbol{B}^+$ is used.

In addition to the equality of INDI with restoring to $\boldsymbol{u}_{\text{des}} = \boldsymbol{0}$ and sNDI, we can show equality for $\boldsymbol{u}_{\text{des}} \neq \boldsymbol{0}$. For sNDI, we recall :

$$\begin{aligned}\boldsymbol{u}_{\text{cmd}} &= \boldsymbol{B}^+\left(\Delta\boldsymbol{\nu}_{\text{des}} + \boldsymbol{B}\boldsymbol{u}_0 - \boldsymbol{B}\boldsymbol{u}_{\text{des}}\right) + \boldsymbol{u}_{\text{des}} \\ &= \boldsymbol{B}^+\Delta\boldsymbol{\nu}_{\text{des}} + \boldsymbol{B}^+\left(\boldsymbol{B}\boldsymbol{u}_0 - \boldsymbol{B}\boldsymbol{u}_{\text{des}}\right) + \boldsymbol{u}_{\text{des}} \\ &= \boldsymbol{B}^+\Delta\boldsymbol{\nu}_{\text{des}} + \boldsymbol{B}^+\boldsymbol{B}\left(\boldsymbol{u}_0 - \boldsymbol{u}_{\text{des}}\right) + \boldsymbol{u}_{\text{des}}. \end{aligned} \tag{81}$$

For INDI, we substitute $\Delta\boldsymbol{u}_{\text{des}} = \boldsymbol{u}_{\text{des}} - \boldsymbol{u}_0$ leading to

$$\begin{aligned}\boldsymbol{u}_{\text{cmd}} &= \boldsymbol{B}^+\Delta\boldsymbol{\nu}_{\text{des}} - \boldsymbol{B}^+\boldsymbol{B}\Delta\boldsymbol{u}_{\text{des}} + \Delta\boldsymbol{u}_{\text{des}} + \boldsymbol{u}_0 \\ &= \boldsymbol{B}^+\Delta\boldsymbol{\nu}_{\text{des}} + \boldsymbol{B}^+\boldsymbol{B}\left(\boldsymbol{u}_0 - \boldsymbol{u}_{\text{des}}\right) + \boldsymbol{u}_{\text{des}} \\ &\quad - \boldsymbol{u}_0 + \boldsymbol{u}_0 \\ &= \boldsymbol{B}^+\Delta\boldsymbol{\nu}_{\text{des}} + \boldsymbol{B}^+\boldsymbol{B}\left(\boldsymbol{u}_0 - \boldsymbol{u}_{\text{des}}\right) + \boldsymbol{u}_{\text{des}}. \end{aligned} \tag{82}$$

By that, equality of INDI and sNDI with restoring to a generic desired input vector is shown if the same $\boldsymbol{B}$ is used in all parts.

REFERENCES

[1] S. Sieberling, Q. P. Chu, and J. A. Mulder, "Robust flight control using incremental nonlinear dynamic inversion and angular acceleration prediction," *J. Guid., Control, Dyn.*, vol. 33, no. 6, pp. 1732–1742, 2010.

[2] J. J. Harris, "F-35 flight control law design, development and verification," in *Proc. Aviation Technol., Integration, Operations Conf.*, Atlanta, GA, USA: American Institute of Aeronautics and Astronautics, Jun. 2018, Art. no. 3516.

[3] P. Smith and A. Berry, "Flight test experience of a non-linear dynamic inversion control law on the VAAC harrier," in *Proc. Atmospheric Flight Mechan. Conf.*, Denver, CO, USA: American Institute of Aeronautics and Astronautics, Aug. 2000, pp. 133–142.

[4] S. A. Raab, J. Zhang, P. Bhardwaj, and F. Holzapfel, "Proposal of a unified control strategy for vertical take-off and landing transition aircraft configurations," in *Proc. Appl. Aerodynamics Conf.*, Reston, VA, USA: American Institute of Aeronautics and Astronautics, 2018, Art. no. 3478.

[5] T. M. L. De Ponti, E. J. J. Smeur, and B. D. W. Remes, "Unified actuator nonlinear dynamic inversion controller for the variable skew quad plane," *J. Guid., Control, Dyn.*, vol. 48, no. 5, pp. 1167–1176, 2025.

[6] E. Smeur, G. de Croon, and Q. Chu, "Cascaded incremental nonlinear dynamic inversion for MAV disturbance rejection," *Control Eng. Pract.*, vol. 73, pp. 79–90, 2018.

[7] T. Rupprecht, A. Steinert, C. Kotitschke, and F. Holzapfel, "INDI control law structure for a MEDEVAC eVTOL and its reference models: Feedforward, physical limitations, and innerloop dynamics for optimal tracking," in *Proc. AIAA Aviation Forum ASCEND Co-Located Conf. Proc.*, Reston, VA, USA: American Institute of Aeronautics and Astronautics, 2024, Art. no. 4425.

[8] A. Steinert, S. Raab, S. Hafner, F. Holzapfel, and H. Hong, "From fundamentals to applications of incremental nonlinear dynamic inversion: A survey on INDI–Part I," *Chin. J. Aeronaut.*, vol. 38, no. 11, Apr. 2025, Art. no. 103553.
[9] A. Steinert, S. Raab, S. Hafner, F. Holzapfel, and H. Hong, "Advancements in incremental nonlinear dynamic inversion and its components: A survey on INDI–Part II," *Chin. J. Aeronaut.*, vol. 38, no. 11, May 2025, Art. no. 103591.
[10] R. Steffensen, A. Steinert, and E. J. J. Smeur, "Nonlinear dynamic inversion with actuator dynamics: An incremental control perspective," *J. Guid., Control, Dyn.*, vol. 46, no. 4, pp. 709–717, 2023.
[11] I. Matamoros and C. C. de Visser, "Incremental nonlinear control allocation for a tailless aircraft with innovative control effectors," in *Proc. AIAA Guid., Navigation, Control Conf.* Reston, VA, USA: American Institute of Aeronautics and Astronautics, 2018, p. 1116.
[12] R. Stolk and C. de Visser, "Minimum drag control allocation for the innovative control effector aircraft," in *Proc. CEAS EuroGNC Conf.*, Milan, Italy, 2019, Art. no. CEAS-GNC-2019-030.
[13] W. Durham, K. A. Bordignon, and R. Beck, *Aircraft Control Allocation*, Somerset, U.K.: John Wiley & Sons Inc, 2016.
[14] W. C. Durham and K. A. Bordignon, "Multiple control effector rate limiting," *J. Guid., Control, Dyn.*, vol. 19, no. 1, pp. 30–37, Jan. 1996.
[15] J. Zhang, P. Bhardwaj, S. A. Raab, S. Saboo, and F. Holzapfel, "Control allocation framework for a tilt-rotor vertical take-off and landing transition aircraft configuration," in *Proc. Appl. Aerodynamics Conf.*, Reston, VA, USA: American Institute of Aeronautics and Astronautics, 2018, Art. no. 3480.
[16] O. Härkegård, "Efficient active set algorithms for solving constrained least squares problems in aircraft control allocation," in *Proc. Proc. 41st IEEE Conf. Decis. Control*, 2002, pp. 1295–1300.
[17] E. Smeur, D. Höppener, and C. D. Wagter, "Prioritized control allocation for quadrotors subject to saturation," in *Proc. Int. Micro Air Veh. Conf. Flight Competition*, 2017, pp. 37–43.
[18] Y. Beyer, M. Steen, and P. Hecker, "Incremental passive fault-tolerant control for quadrotors subjected to complete rotor failures," *J. Guid., Control, Dyn.*, vol. 46, no. 10, pp. 2033–2042, Oct. 2023.
[19] D. Milz and G. Looye, "Tilt-wing control design for a unified control concept," in *Proc. AIAA SCITECH 2022 Forum*. Reston, VA, USA: American Institute of Aeronautics and Astronautics, 2022, Art. no. 1084.
[20] D. Milz, M. May, and G. Looye, "Dynamic inversion-based control concept for transformational tilt-wing eVTOLs," in *Proc. AIAA Scitech 2024 Forum*. Orlando, FL, USA: AIAA, Jan. 2024, Art. no. 1290.
[21] D. Milz, M. S. May, and G. Looye, "Tandem tilt-wing control design based on sensory nonlinear dynamic inversion," in *Proc. AIAA Aviation Forum ASCEND 2024*. Las Vegas, NV, USA: American Institute of Aeronautics and Astronautics, Jul. 2024, Art. no. 4418.
[22] A. Mancinelli, B. D. W. Remes, G. C. H. E. De Croon, and E. J. J. Smeur, "Real-time nonlinear control allocation framework for vehicles with highly nonlinear effectors subject to saturation," *J. Intell. Robotic Syst.*, vol. 108, no. 4, Aug. 2023, Art. no. 67.
[23] D. Milz, M. S. May, and G. Looye, "Flight testing air data sensor failure handling with hybrid nonlinear dynamic inversion," in *Proc. CEAS EuroGNC Conf.*, Bristol, U.K., 2024, Art. No. CEAS-GNC-2024-082.
[24] D. Milz, M. May, and G. Looye, "Tandem tilt-wing control law design using hybrid nonlinear dynamic inversion," *J. Guid., Control, Dyn.*, pp. 1–9, Jan. 2026.
[25] J.-J. E. Slotine and W. Li, *Applied Nonlinear Control*. Englewood Cliffs, NJ, USA: Prentice Hall, 1991.
[26] F. Holzapfel, "Nichtlineare adaptive regelung eines unbemannten fluggerätes," Ph.D. dissertation, Technischen Universität, München, München, Germany, 2004.
[27] B. Bacon and A. Ostroff, "Reconfigurable flight control using nonlinear dynamic inversion with a special accelerometer implementation," in *Proc. AIAA Guid., Navigation, Control Conf. Exhibit*. Denver, CO, USA: American Institute of Aeronautics and Astronautics, 2000, Art. no. 4565.
[28] T. De Ponti, S. F. Hafner, and E. Smeur, "Test data on the equivalence of sensory and incremental nonlinear dynamic inversion." 4TU.ResearchData, Jul. 2025, doi: 10.4121/00c545c3-4fe3-4a1f-b918-20f430231fb6.v1.
[29] W. C. Durham, "Constrained control allocation," *J. Guid., Control, Dyn.*, vol. 16, pp. 711–725, 1993.
[30] D. Enns, "Control allocation approaches," in *Proc. Guid., Navigation, Control Conf. Exhibit*. Boston, MA, USA: American Institute of Aeronautics and Astronautics, Aug. 1998, pp. 98–108.
[31] T. M. L. De Ponti, E. J. J. Smeur, and B. W. D. Remes, "Incremental nonlinear dynamic inversion controller for a variable skew quad plane," in *Proc. Int. Conf. Unmanned Aircr. Syst.*, Jun. 2023, pp. 241–248.

SIMON HAFNER (Graduate Student Member, IEEE) received the B.Sc. degree in mechanical engineering and the M.Sc. degree in mechatronics and robotics from the Technical University of Munich, Munich, Germany, in 2020 and 2021, respectively. He is currently working toward the Ph.D. degree in aerospace engineering with the Institute of Flight System Dynamics, Technical University of Munich, Germany. His research interests include flight control algorithms, specifically incremental nonlinear dynamic inversion, control allocation, and adaptive control allocation. He specifically focuses on reducing the execution time of control allocation algorithms. He was the recipient of the Ph.D. scholarship from Munich Aerospace e.V. from 2022 to 2025 for the Ph.D. studies.

TOMASO DE PONTI received the B.Sc. and M.Sc. degrees in aerospace engineering from the Delft University of Technology (TU Delft), Delft, The Netherlands, in 2019 and 2022, respectively. He is currently working toward the Ph.D. degree in aerospace engineering with the Department of Control and Simulation, Faculty of Aerospace Engineering, Delft University of Technology, The Netherlands. His Ph.D. research is conducted in collaboration with the Royal Netherlands Navy and the Netherlands Coast Guard. His work focuses on fault-tolerant flight control and on extending these control methods to more accurately capture actuator dynamics within the control law. His research interests include the application of incremental control laws, such as Incremental Nonlinear Dynamic Inversion (INDI) and Actuator Nonlinear Dynamics Inversion (ANDI), to unconventional aerial systems such as the Variable Skew Quad Plane.

EWOUD SMEUR received the B.Sc., M.Sc. and Ph.D. degrees in aerospace engineering from the Delft University of Technology, Delft, The Netherlands, in 2011, and 2014 and 2018 respectively. He is currently an Assistant Professor with the department of Control and Simulation, Faculty of Aerospace Engineering, Delft University of Technology. In 2019, he was a Postdoc with the Institute of Flight System Dynamics, Technical University of Munich, Germany. His research interest includes the development of flight control laws such as INDI for novel types of UAVs, hybrid drones, novel sensors, and navigation solutions.